

Massive Milky Way Satellites in Cold and Warm Dark Matter: Dependence on Cosmology

E. Polisensky^{1*} and M. Ricotti^{2,3*†}

¹*Naval Research Laboratory, Washington, D.C. 20375, USA*

²*Department of Astronomy, University of Maryland, College Park, Maryland 20745, USA*

³*Sorbonne Universités, Institut Lagrange de Paris (ILP), 98 bis Boulevard Arago 75014 Paris, France*

1 October 2018

ABSTRACT

We investigate the claim that the largest subhaloes in high resolution dissipationless cold dark matter (CDM) simulations of the Milky Way are dynamically inconsistent with observations of its most luminous satellites. We find that the inconsistency is largely attributable to the large values of σ_8 and n_s adopted in the discrepant simulations, producing satellites that form too early and therefore are too dense. We find the tension between observations and simulations adopting parameters consistent with WMAP9 is greatly diminished, making the satellites a sensitive test of CDM. We find the Via Lactea II halo to be atypical for haloes in a WMAP3 cosmology, a discrepancy that we attribute to its earlier formation epoch than the mean for its mass. We also explore warm dark matter (WDM) cosmologies for 1–4 keV thermal relics. In 1 keV cosmologies subhaloes have circular velocities at kpc scales $\sim 60\%$ lower than their CDM counterparts, but are reduced by only 10% in 4 keV cosmologies. Since relic masses $< 2\text{--}3$ keV are ruled out by constraints from the number of Milky Way satellites and Lyman- α forest, WDM has a minor effect in reducing the densities of massive satellites. Given the uncertainties on the mass and formation epoch of the Milky Way, the need for reducing the satellite densities with baryonic effects or WDM is alleviated.

Key words: galaxies: haloes, dwarf, cosmology: theory

1 INTRODUCTION

The satellite galaxies of the Milky Way (MW), being the closest extragalactic objects and indeed within the virial radius of the Milky Way's extended halo of dark matter, are uniquely suited for testing theories of galaxy formation and evolution and the nature of dark matter. The MW satellites known before the Sloan Digital Sky Survey (SDSS) numbered too few to account for predictions from N-body simulations in Λ CDM cosmologies that were otherwise successful in describing the abundances of galaxies in clusters and the large scale features of the matter distribution (Klypin et al. 1999; Moore et al. 1999). The discovery of a population of fainter satellites in the SDSS and more sophisticated simulations that account for supernova feedback and the heating of the intergalactic medium (IGM) during reionization have alleviated this problem by predicting a strong suppression of galaxy formation

in low mass haloes (Bullock, Kravtsov & Weinberg 2000; Ricotti, Gnedin & Shull 2002a,b, 2008).

Recent work focusing on the brightest MW satellites has highlighted dynamical discrepancies with high-resolution CDM simulations. Boylan-Kolchin, Bullock & Kaplinghat (2011, 2012) compared the most luminous satellites to subhaloes in the Aquarius simulation suite of six Milky Way-sized haloes. Abundance matching models set a one-to-one correspondence between luminosity and dynamical mass and place the brightest satellites in the largest subhaloes. However, the observed stellar velocities cannot be reconciled with the velocity profiles of the largest dark matter subhaloes in simulation. The most massive satellites, either at the present epoch, the epoch of reionization, or over the complete infall history, are too dense to be dynamically consistent with the Milky Way satellites. Observations of the stellar velocity dispersions in the bright satellites are consistent with dark matter haloes with maximum circular velocities $< 25 \text{ km s}^{-1}$ while the Aquarius Milky Ways have about 10 subhaloes each with $v_{max} > 25 \text{ km s}^{-1}$ that are also not Magellenic Cloud analogues. Several solutions to this problem have been

* E-mail: Emil.Polisensky@nrl.navy.mil

† E-mail: ricotti@astro.umd.edu

proposed. Galaxy formation may be stochastic on dwarf spheroidal scales and the bright satellites do not reside in the largest subhaloes (Boylan-Kolchin, Bullock & Kaplinghat 2011; Katz & Ricotti 2012). This requires abandoning the monotonic relation between galaxy luminosity and halo mass that is well-established for brighter galaxies.

Interestingly, in models in which some of the ultra-faint dwarfs are fossils of the first galaxies (Ricotti & Gnedin 2005; Bovill & Ricotti 2009), show some tension with observations only at the bright end of the satellite luminosity function (Bovill & Ricotti 2011a,b). Simulations that produce a numerous population of ultra-faint dwarfs also produce an overabundance of bright dwarf satellites especially in the outer parts of the Milky Way. However, this tension is eased by the expected stripping of the extended primordial stellar population around bright satellites.

The number of satellites of all size are known to be proportional to the mass of the host halo (Klypin et al. 1999). Wang et al. (2012) argue the low velocities of the MW satellites may be an indication the MW is less massive than typically thought. They show there is only a 5% probability for a galaxy of mass $2 \times 10^{12} M_{\odot}$ to have 3 satellites or less with maximum circular velocities $> 30 \text{ km s}^{-1}$ but 40% for a galaxy of mass $10^{12} M_{\odot}$. A low mass for the Milky Way of $8 \times 10^{11} M_{\odot}$ is also favored in the work of Vera-Ciro et al. (2013). Direct measures of the MW mass typically focus on stellar tracers of the inner halo or radial velocity measurements of the MW satellites and give a range of virial mass $0.8 - 2.5 \times 10^{12} M_{\odot}$, we refer the reader to the references in Boylan-Kolchin et al. (2012) where observations of the spatial motion of Leo I are used to constrain the mass of the Milky Way to $> 10^{12} M_{\odot}$ at 95% confidence.

Sawala et al. (2012) show the simulations can be reconciled with the observations by including baryonic physics in the simulations. Inclusion of baryonic physics removes gas from haloes through supernova expulsion of the interstellar medium, prevention of gas accretion through reionization heating of the IGM, and ram pressure stripping from satellites. Removal of baryons from the dark matter haloes also reduces the potential well resulting in less accretion of both gas and dark matter. They show dark matter only simulations overpredict the subhalo abundance by 30% at a mass scale of $10^{10} M_{\odot}$ with an increasing number of subhaloes with no gas or stars below this scale.

The influence of baryons was also studied by di Cintio et al. (2011). They found that while satellites with low baryon fractions have lower concentrations than their dark matter only counterparts, satellites with high baryon fractions have higher central densities due to adiabatic contraction. Satellites with high baryon fractions also tend to have the largest maximum circular velocities. However, their recent work (Di Cintio et al. 2013) finds the subhalo density profiles are better described by Einasto profiles than Navarro, Frenk, and White (NFW) profiles (Navarro, Frenk & White 1997) and that this reconciles the observations with simulated satellites of similar luminosities. Vera-Ciro et al. (2013) also find agreement with Einasto profiles. However, while the initial work of Boylan-Kolchin, Bullock & Kaplinghat (2011) assumes NFW profiles their later work (Boylan-Kolchin, Bullock & Kaplinghat 2012) uses the

subhalo circular velocity profiles directly with no assumed form.

Another possibility is a change in the nature of the dark matter from standard CDM assumptions of collisionless particles with low intrinsic thermal velocities. Vogelsberger, Zavala, & Loeb (2012) simulated one of the Aquarius Milky Way haloes in self-interacting dark matter models. The ability of the dark matter particles to self-scatter leads to the formation of subhaloes with constant density cores. The lower density decreases the inner circular velocity profiles bringing the simulations into agreement with the observations.

A truncation in the dark matter power spectrum was investigated as a solution to the paucity of satellites by reducing the abundance of haloes at subgalactic scales. One method for producing a truncated power spectrum is if the dark matter particles decoupled with relativistic velocities early in the radiation dominated era and thereby able to stream out of overdense regions before becoming nonrelativistic at a time before the horizon had reached Galactic scales. The scale of the power spectrum truncation in ‘warm’ dark matter (WDM) is related to the mass of the dark matter particle with lighter particles decoupling earlier and able to stream longer.

Dwarf-scale haloes in WDM cosmologies form later and have lower concentrations than haloes in CDM, offering a potential solution to the dynamical discrepancies. Lovell et al. (2012) simulated one of the Aquarius haloes in a 1 keV thermal relic WDM cosmology and showed the subhaloes have central densities and velocity profiles in agreement with the bright MW satellites. In Lovell et al. (2013) their work was extended to particle masses 1.4-2.3 keV. Recently, one Milky Way-like halo was simulated in WDM at 2, 3, and 4 keV (Schneider et al. 2013). In this work we investigate the subhalo dynamics in four Milky Way-sized haloes in 1, 2, 3, and 4 keV cosmologies.

Another area potentially affecting the subhalo densities are the adopted cosmological parameters. The Via Lactea II (VL2) simulation (Diemand, Kuhlen & Madau 2007; Diemand et al. 2008), which adopted parameters from the 3rd year release of the *Wilkinson Microwave Anisotropy Probe* (WMAP), was found to give similar results as the six Aquarius haloes adopting WMAP1 parameters. However, reason to suspect the adopted cosmology is important comes from Macciò, Dutton & van den Bosch (2008) who explored the dependence of halo concentration on the adopted cosmological model for field galaxies. They fit NFW density profiles to the haloes in their simulations:

$$\rho(r) = \frac{\delta_c \rho_{crit}}{(r/r_s)(1+r/r_s)^2}, \quad (1)$$

and determined the concentrations, $c_{200} = R_{200}/r_s$, where R_{200} is the radius enclosing a density 200 times the critical density, ρ_{crit} . They found the average concentration of dwarf-scale field haloes varies by a factor of 1.55 between WMAP1 and WMAP3. In this work we also examine the dependence of our CDM subhalo populations on the adopted cosmological parameters.

2 SIMULATIONS

All our simulations were conducted with the N -body cosmological simulation code GADGET-2 (Springel 2005) with gravitational physics only and initial conditions generated with the GRAFIC2 software package (Bertschinger 2001). We use the high resolution simulations presented in Polisensky & Ricotti (2011) where two Milky Way-sized haloes were simulated in a cubic box with comoving side length of 90 Mpc, mass resolution of $9.2 \times 10^4 M_\odot$, and a 275 pc gravitational softening length. We refer to these haloes as the *set A* and *set B* simulations. We also ran a high resolution simulation of halo *C8* from Polisensky & Ricotti (2011) with a 138 pc softening length and refer to this as our *set C* simulations. Finally, we ran an additional *set D* simulation of another Milky Way-sized halo in a 67 Mpc comoving box with a mass resolution $8.2 \times 10^4 M_\odot$ and gravitational softening length 196 pc.

Table 1 lists sets of cosmological parameters from measurements of the cosmic microwave background by WMAP and the *Planck* mission (Spergel et al. 2003, 2007; Komatsu et al. 2009; Larson et al. 2010; Jarosik et al. 2010; Komatsu et al. 2011; Hinshaw et al. 2012; Planck Collaboration et al. 2013). “Bolshoi” are the parameters from the Bolshoi simulation (Klypin, Trujillo-Gomez & Primack 2011) which were chosen to be within 1σ of WMAP5, WMAP7, and consistent with the results of supernovae, and X-ray cluster surveys. These parameters are within 1σ of WMAP9 except the value of n_s which is within 1.7σ . They are also within 1.2σ of Planck1 with the exceptions of Ω_m and Ω_Λ which are 2.2σ below Planck1. The WMAP1 parameters are $2.4 - 4.1\sigma$ away from Planck1 while σ_8 and n_s are 3.4σ and 2.2σ above WMAP9, respectively. In contrast, the value of σ_8 in WMAP3 is 3.5σ below WMAP9 and Planck1.

Figure 1 shows the linear power spectra for the parameters listed in Table 1 normalized by the Bolshoi power spectrum. On the scale of the dwarfs ($k \sim 10 \text{ Mpc}^{-1}$) the power varies greatly across cosmologies with WMAP1 and WMAP3 representing the extremes of high and low power. The Bolshoi parameters, however, represent a conservative estimate of the power on dwarf scales while being consistent with the latest CMB measurements from WMAP and *Planck*.

To investigate the dependence of satellite densities on cosmology we ran CDM simulations for each of our four sets adopting WMAP1, WMAP3, and Bolshoi parameters with the CDM transfer function from Eisenstein & Hu (1998). The box size and softening lengths were scaled in each simulation to keep the mass resolution constant. A series of low resolution tests of the *set B* halo were also run, these are described in the next section.

For our investigation of warm dark matter we used the warm dark matter transfer function given by Bode, Ostriker, & Turok (2001) valid for particles in thermal equilibrium at the time of their decoupling, such as the gravitino. We adopted Bolshoi parameters and ran simulations for particle masses of 1, 2, 3, and 4 keV for each halo.

We used version 1.0 of the AMIGA’s Halo Finder (AHF) software (Knollmann & Knebe 2009) to identify the Milky Way haloes and their gravitationally bound subhaloes after iteratively removing unbound particles. Table 2 summarizes

Table 1. Cosmological parameters.

Name	Ω_m	Ω_Λ	Ω_b	h	σ_8	n_s
WMAP1	0.25	0.75	0.045	0.73	0.90	1.0
WMAP3	0.238	0.762	0.040	0.73	0.74	0.951
WMAP5	0.258	0.742	0.0441	0.72	0.796	0.963
WMAP7	0.267	0.733	0.0449	0.71	0.801	0.963
WMAP9	0.282	0.718	0.0461	0.70	0.817	0.964
Planck1	0.317	0.683	0.0486	0.67	0.834	0.962
Bolshoi	0.27	0.73	0.0469	0.70	0.82	0.95

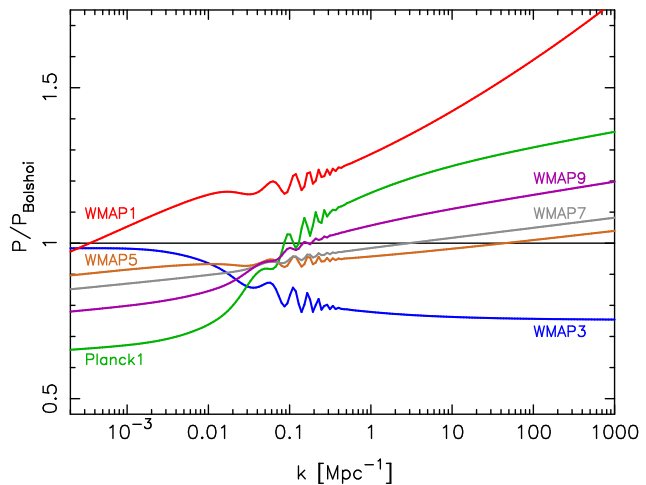


Figure 1. Power spectra for CDM cosmologies normalized by the Bolshoi power spectrum.

the properties calculated by AHF for our simulated Milky Ways at $z = 0$. We write R_{100} to mean the radius enclosing an overdensity 100 times ρ_{crit} . The mass and number of particles inside R_{100} are M_{100} and N_{100} , respectively; $v_{max} = \max(v_{circ})$ is the maximum circular velocity of the halo occurring at a radius R_{max} , and $v_{circ}^2 = GM(< r)/r$. Also given is the NFW c_{200} concentration for each halo determined from:

$$\left(\frac{v_{max}}{v_{200}}\right)^2 = 0.2162 c_{200}/f(c_{200}), \quad (2)$$

where $f(c) = \ln(1+c) - c/(1+c)$.

We also ran the SUBFIND program (Springel et al. 2001) on the *set B* WMAP3 data and found excellent agreement with the results from AHF.

We saved snapshots of the particle information every 0.05 change in the universal scale factor, $a = (1+z)^{-1}$, for simulations adopting Bolshoi and WMAP1 parameters. Figure 2 shows the mass growth of each of our MW haloes and the VL2 halo as a function of a . The masses are normalized to the halo mass at $a = 1$. The MergerTree tool in AHF was used to construct merger trees for all identified haloes. This allows determination of v_{infall} for each subhalo, the maximum value of v_{max} over a halo’s formation and accretion history: $v_{infall} = \max(v_{max}(z))$. We follow the work of Boylan-Kolchin, Bullock & Kaplinghat (2011) and consider subhaloes within 300 kpc of our Milky Way centres. We similarly identify subhaloes with $v_{max} > 40 \text{ km s}^{-1}$ and $v_{infall} > 60 \text{ km s}^{-1}$ as hosts of Magellanic Cloud analogues.

Table 2. Properties of simulations and Milky Way haloes at $z = 0$.

Cosmology		m_{res} [M_{\odot}]	M_{100} [$10^{12} M_{\odot}$]	R_{100} [kpc]	v_{max} [km s $^{-1}$]	R_{max} [kpc]	N_{100}	c_{200}
<i>Set A</i>								
CDM	WMAP1	9.17×10^4	2.1119	324.233	214.78	39.849	23,028,026	9.68
CDM	Bolshoi	9.17×10^4	1.9803	326.357	198.97	55.243	21,560,499	8.38
CDM	WMAP3	9.17×10^4	1.8410	309.740	192.28	41.027	20,074,556	7.77
4 keV	Bolshoi	9.17×10^4	1.9644	325.486	198.11	50.414	21,387,017	8.25
3 keV	Bolshoi	9.17×10^4	1.9724	325.929	197.05	54.900	21,474,003	7.99
2 keV	Bolshoi	9.17×10^4	2.0061	327.771	197.54	39.871	21,874,542	7.96
1 keV	Bolshoi	9.17×10^4	2.0197	328.514	199.24	58.943	22,022,816	8.04
<i>Set B</i>								
CDM	WMAP1	9.17×10^4	2.0873	322.973	210.02	67.068	22,760,127	9.01
CDM	Bolshoi	9.17×10^4	1.9271	323.414	194.90	82.086	21,012,806	7.81
CDM	WMAP3	9.17×10^4	1.7540	304.781	194.62	79.767	19,125,479	8.29
4 keV	Bolshoi	9.17×10^4	1.9193	322.971	194.19	74.900	20,928,496	7.69
3 keV	Bolshoi	9.17×10^4	1.9224	323.157	193.65	77.500	20,962,535	7.64
2 keV	Bolshoi	9.17×10^4	1.9242	323.257	194.53	79.500	20,981,724	7.90
1 keV	Bolshoi	9.17×10^4	1.8804	320.771	195.23	84.286	20,503,730	8.06
<i>Set C</i>								
CDM	WMAP1	9.17×10^4	2.4195	339.274	231.42	44.932	26,240,319	11.13
CDM	Bolshoi	9.17×10^4	2.3259	344.343	215.81	58.943	25,211,233	9.05
CDM	WMAP3	9.17×10^4	1.9887	317.808	203.42	56.164	21,645,271	8.72
4 keV	Bolshoi	9.17×10^4	2.3195	344.029	215.03	56.900	25,152,203	8.95
3 keV	Bolshoi	9.17×10^4	2.3194	344.014	215.25	57.100	25,153,016	9.01
2 keV	Bolshoi	9.17×10^4	2.3113	343.614	214.40	61.529	25,070,237	8.88
1 keV	Bolshoi	9.17×10^4	2.2607	341.086	210.94	64.857	24,563,114	8.61
<i>Set D</i>								
CDM	WMAP1	8.21×10^4	1.8164	308.342	190.95	67.027	22,135,114	7.29
CDM	Bolshoi	8.21×10^4	1.5944	303.614	176.26	69.057	19,429,510	6.80
CDM	WMAP3	8.21×10^4	1.2575	272.781	164.27	50.164	15,323,846	6.56
4 keV	Bolshoi	8.21×10^4	1.5930	303.526	176.62	75.414	19,412,993	6.77
3 keV	Bolshoi	8.21×10^4	1.5875	303.171	176.38	74.143	19,345,715	6.78
2 keV	Bolshoi	8.21×10^4	1.5548	301.086	175.73	75.729	18,947,343	6.81
1 keV	Bolshoi	8.21×10^4	1.4998	297.486	171.97	79.514	18,276,956	6.39
<i>Set B Low Resolution Tests</i>								
CDM	WMAP1	7.34×10^5	2.3249	334.795	221.67	68.795	3,168,819	9.56
CDM sm	WMAP1	5.92×10^5	1.8899	312.452	208.53	73.630	3,192,628	9.92
CDM sm hi z_i	WMAP1	5.92×10^5	1.9162	313.890	212.12	66.233	3,237,093	10.63
CDM	Planck1	7.34×10^5	2.3463	355.582	215.70	71.209	3,198,000	10.02
CDM	WMAP9	7.34×10^5	2.1919	337.600	210.15	78.429	2,987,609	9.29
CDM	Bolshoi	7.34×10^5	2.0793	331.714	205.26	77.943	2,834,081	8.91
CDM	WMAP3	7.34×10^5	1.7650	305.411	191.01	98.288	2,405,721	7.45
CDM hi z_i	WMAP3	7.34×10^5	1.9375	315.055	198.24	82.740	2,640,759	7.92

We compare our simulated subhaloes to the MW dwarf spheroidal satellites with luminosities $L_V > 10^5 L_{\odot}$. Walker et al. (2009) and Wolf et al. (2010) show line-of-sight velocity measurements provide good constraints on the dynamical masses of dispersion-supported galaxies like the MW dwarfs spheroidals. The Magellanic Clouds are excluded from our observation sample as they are irregular type galaxies. The Sagittarius dwarf is also excluded because it is undergoing disruption and far from equilibrium. Our observed sample consists of nine galaxies: Canes Venatici I,

Carina, Draco, Fornax, Leo I, Leo II, Sculptor, Sextans, and Ursa Minor.

3 RESULTS

3.1 Cold Dark Matter

Figure 3 is a plot of v_{max} and R_{max} for subhaloes in our high resolution CDM simulations.

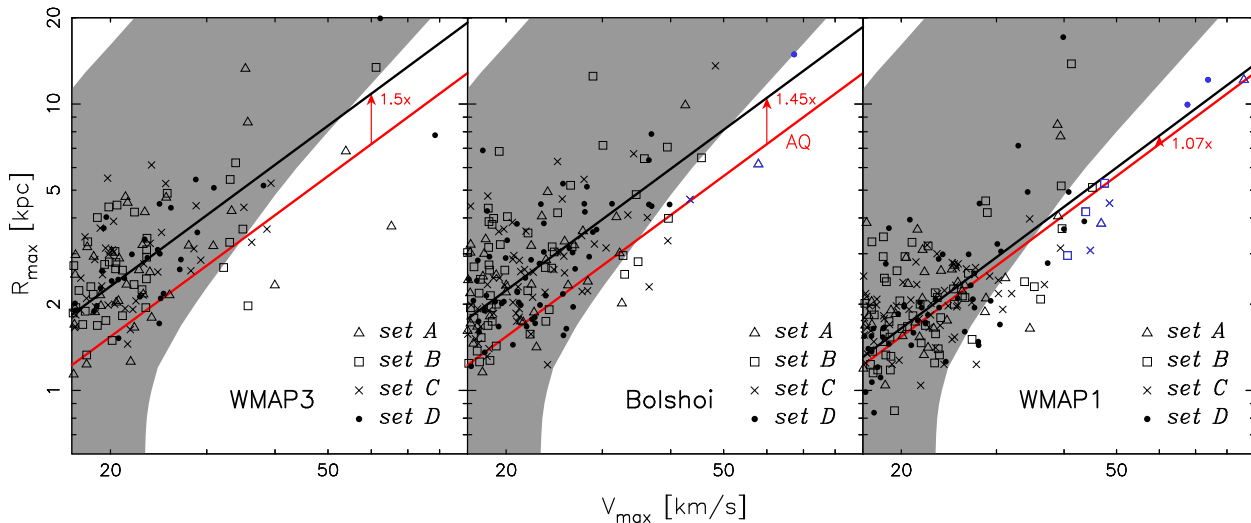


Figure 3. Plots of v_{max} and R_{max} for subhaloes in the high resolution CDM simulations for each set of cosmological parameters. The shaded area shows the 2σ constraints for the bright Milky Way dwarfs from Boylan-Kolchin, Bullock & Kaplinghat (2011) assuming NFW profiles. The sloped red line shows the mean of the Aquarius subhaloes. Magellanic Cloud analogues in the Bolshoi and WMAP1 simulations are plotted in blue.

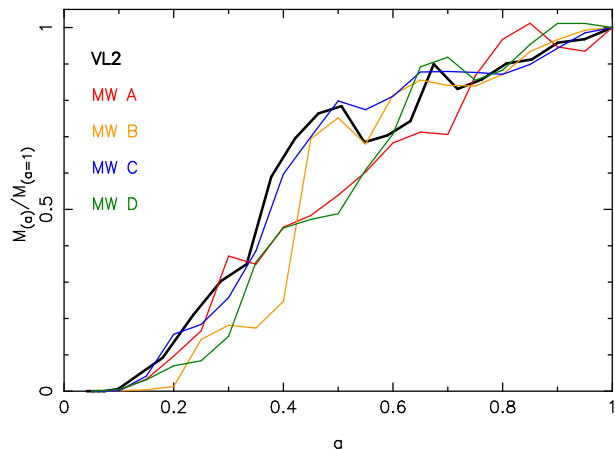


Figure 2. Mass growth histories of simulated Milky Way haloes as a function of scale factor, a .

Boylan-Kolchin, Bullock & Kaplinghat (2011) investigated what values of v_{max} and R_{max} of NFW haloes (Navarro, Frenk & White 1997) are consistent with the half-light dynamical mass constraints of the bright MW dwarf spheroidals from Wolf et al. (2010). Their 2σ confidence region is plotted as the shaded regions in Figure 3.

We see there are many subhaloes that lie in the range consistent with the MW dwarfs, but there are some with $v_{max} > 20 \text{ km s}^{-1}$ that do not. These are the subhaloes highlighted by Boylan-Kolchin, Bullock & Kaplinghat (2011) that are massive but have central densities too high to host any of the MW dwarfs. However our WMAP3 and Bolshoi simulations have only 1-3 subhaloes per parent halo outside the shaded zone of Milky Way satellites compared to 4-8 subhaloes for the WMAP1 simulations. This is due to R_{max} being shifted to higher values from WMAP1 for the same values of v_{max} .

Springel et al. (2008) show that the logarithms of v_{max}

and R_{max} for the Aquarius subhaloes have a linear relationship. We estimate the equation of their fitting line:

$$\log R_{max} = 1.41 \log(v_{max}/14.72 \text{ km s}^{-1}), \quad (3)$$

and plot this as the red line. We assumed a constant slope and performed least-squares fits to our subhaloes in each cosmology and plot these as the black lines. The red arrowed lines show the shift in R_{max} for each of our simulation sets compared to Aquarius. Our simulations adopting WMAP1 parameters are in good agreement with the Aquarius simulations, differing by only a factor of 1.07, but in Bolshoi and WMAP3 the subhaloes are offset to higher values of R_{max} by factors of 1.45 and 1.50, respectively.

We compared the fit for each simulation set separately to the corresponding fit in the WMAP1 cosmology. We found the average scale in R_{max} from WMAP1 to Bolshoi is a factor of 1.35 and a factor of 1.40 for WMAP3, with a 1σ scatter of ± 0.10 for each.

To determine if factors other than the cosmology may be affecting the subhalo densities we ran a series of tests on the *set B* halo with the mass resolution decreased a factor of 8 but the softening length kept the same as the high resolution simulations. We ran a test adopting WMAP3 parameters starting from the same initial redshift as the high resolution simulation ($z_i = 48$) and another test starting from a high redshift ($z_i = 115$), comparable to the starting redshift of Aquarius ($z_i = 127$). We also ran tests adopting the WMAP1 parameters. The Milky Way halo mass was about 30% greater in this simulation so we ran tests with the box size and mass resolution decreased to give a halo mass similar to the WMAP3 tests. We ran small box tests starting from the same low and high redshifts.

We examined applying velocity cuts of $v_{max} > 14 - 20 \text{ km s}^{-1}$ to the subhaloes. At smaller velocities the R_{max} values for some subhaloes were inside the convergence radius satisfying the criterion of Power et al. (2003) and therefore affected by the resolution of the simulations. In Figure 4 we normalize the values of R_{max} for all subhaloes

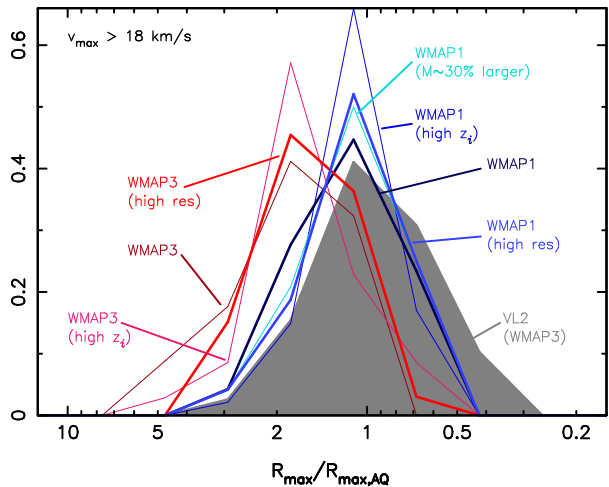


Figure 4. Distribution functions of R_{max} normalized to the Aquarius values for CDM subhaloes with $v_{max} > 18 \text{ km s}^{-1}$ in the WMAP1 and WMAP3 simulations of the *set B* halo. Simulations adopting WMAP3 parameters are plotted in red while WMAP1 simulations are plotted in blue. The offset between simulations is consistent with a cosmology dependence and not on mass resolution, starting redshift, or mass of the host Milky Way halo. Solid gray area is the distribution for Via Lactea-II subhaloes.

with $v_{max} > 18 \text{ km s}^{-1}$ to the Aquarius value of R_{max} from Equation 3 and present binned distributions for these subhaloes and those of the Via Lactea-II (VL2) simulation ($z_i = 104$). We find consistent distributions between the low and high resolution simulations showing our mass resolution and softening length are sufficient to sample subhaloes with $v_{max} > 18 \text{ km s}^{-1}$. We also find weak to no dependence on the starting redshift as the simulations started from $z_i = 115$ have distributions consistent with the corresponding simulations started from $z_i = 48$. However, we do see a strong dependence on the cosmology as the WMAP3 simulations are offset to higher R_{max} compared to WMAP1. The offset is only weakly dependent on the mass of the Milky Way host as the WMAP1 simulations in the large and small boxes have nearly identical distributions.

We ran additional low resolution tests of the *set B* halo adopting WMAP9, Bolshoi, and Planck1 parameters. These simulations also show offsets from WMAP1 but less than the WMAP3 tests (final column in Table 3), as expected for the greater small scale power in these cosmologies. These tests show the subhalo concentrations are largely determined by their formation time. As the small scale power increases formation occurs earlier and the subhaloes are more concentrated at $z = 0$. This is supported by examining the high redshift data for these simulations. Table 3 gives the number of haloes with masses $> 2 \times 10^8 M_\odot$ and the average mass of the 12 largest haloes in the high resolution volume at $z = 9$ in the test simulations of the *set B* halo with mass resolution $7.34 \times 10^5 M_\odot$. In the high resolution volume at $z = 9$ there are more than six times as many haloes with masses $> 2 \times 10^8 M_\odot$ in the WMAP1 simulation than in WMAP3. Furthermore, the 12 most massive haloes are an average of four times as massive in WMAP1 than WMAP3. This is evidence dwarf-scale haloes are collapsing earlier and have more time to grow in a WMAP1 cosmology.

Table 3. Comparison of the low resolution CDM tests of the *set B* halo with a common mass resolution. See text for an explanation of quantities in the columns.

Name	$N_{z=9}$ $> 2 \times 10^8 M_\odot$	$\langle M_{top12} \rangle$ $[10^9 M_\odot]$	$\frac{R_{max}}{R_{max,WMAP1}}$
WMAP1	378	2.939	1.0
Planck1	239	1.982	1.06
WMAP9	193	1.612	1.16
Bolshoi	149	1.375	1.20
WMAP3	57	0.777	1.57

The distribution of VL2 subhaloes is also plotted in Figure 4. The VL2 simulation used WMAP3 cosmology but its subhaloes have concentrations consistent with Aquarius. We hypothesize this is because the VL2 halo has a higher redshift of formation than the mean for a WMAP3 cosmology. Figure 2 shows our haloes generally have accreted less of their final mass at $a < 0.5$ than the VL2 halo. For example, at $a = 0.25$ the VL2 halo has 23% of its final mass while our haloes have only 5 – 18% of their final masses. Further evidence comes from the halo concentration which is known to correlate with formation epoch. We determined M_{200} and R_{200} ($1.417 \times 10^{12} M_\odot$, 225.28 kpc) from the fit to the VL2 density profile (Diemand et al. 2008) and calculate c_{200} from Eqn 2. The concentration of VL2 is 10.7, in contrast with the 6.6 – 8.7 concentrations of our WMAP3 haloes. VL2 is a 2.4σ outlier in the WMAP3 simulations of Macciò, Dutton & van den Bosch (2008) where the average concentration of relaxed $10^{12} M_\odot h^{-1}$ haloes is 5.9.

3.1.1 Velocity profiles

A direct comparison of the subhalo circular velocity profiles to the half-light circular velocities of the observed dwarfs is desirable but is complicated by two effects. The circular velocity is a cumulative quantity and its profile is affected by the softening length to greater distances than the density profile (Zolotov et al. 2012) making reliable inward extrapolation difficult. Additionally, the hosts of the bright dwarfs are expected to be the largest subhaloes over the complete infall history of the subhalo population or the largest at the epoch of reionization. Many of these subhaloes will experience tidally stripped mass loss thereby reducing their R_{max} sufficiently to become affected by the softening length. The largest subhaloes at present ($z = 0$) are generally subhaloes just beginning to infall as indicated by their large spatial extent (Anderhalden et al. 2013). They are the least affected by stripping and therefore have the most reliable circular velocities. Excluding Magellanic Cloud analogues from our simulations, 5-6 of the 10 subhaloes with greatest v_{max} at $z = 0$ are among the top 10 with greatest v_{infall} while 2-4 are among the top 10 with greatest v_{max} at $z = 9$. Thus while we do not expect the largest subhaloes at $z = 0$ to completely match the observed dwarf population they are useful for illustrating the effects of cosmology on the too big to fail problem.

In Figure 5 we plot the NFW circular velocity profiles with R_{max} and v_{max} values of the 10 largest subhaloes in each CDM simulation adopting WMAP1 and Bolshoi cos-

mologies. The data points with error bars show the circular velocities at half light radii of our bright Milky Way dwarfs sample from Wolf et al. (2010). While there is some halo-to-halo scatter the reduced densities and shift of the profiles to larger radii in the Bolshoi cosmology is dramatically clear.

3.2 Warm Dark Matter

Our results in the previous section show the discrepancy between the largest subhaloes in CDM simulations and observations of bright Milky Way dwarfs may largely be due to the adopted cosmological parameters of the Aquarius simulation and that adopting parameters in agreement with the most recent WMAP release would greatly alleviate this problem. However we also saw that even a WMAP3 simulation like VL2 can have massive satellites dynamically inconsistent with the bright dwarfs implying a dependence on the formation history of the Milky Way and its satellites. In this section we investigate the effects warm dark matter has on the massive subhaloes.

Figure 6 is a plot of v_{max} and R_{max} for subhaloes in each simulation set for each WDM cosmology. Again we see there are many subhaloes that lie in the area consistent with the MW dwarfs but there are some with $v_{max} > 20 \text{ km s}^{-1}$ that do not, however the number of outliers decreases as the particle mass decreases. We find an average of 2 subhaloes per simulation are outside the allowed region decreasing to 1.5 per simulation in 3 keV, < 1 in 2 keV, and 0 in 1 keV. We found an average of 2 subhalo outliers per Bolshoi CDM simulation demonstrating the minimal effect a 4 keV cosmology has on the densities.

The effects of WDM are a reduction in the total number of subhaloes as well as their circular velocities and an increase in their R_{max} . We estimate the increase in R_{max} by fitting equations of the form of Eqn 3 to the WDM subhalo data and comparing to the fits for the corresponding CDM simulation. We find, for constant values of v_{max} , R_{max} values are increased an average of 7% in 4 keV, 15% in 3 keV, 30% in 2 keV, and 46% in 1 keV; however, the small number of subhaloes in 1 keV makes it difficult to achieve a reliable estimate for this cosmology.

We estimate the effects of WDM on the circular velocities by comparing the velocities at several radii in the range 1 – 3 kpc for subhaloes in WDM compared to the corresponding CDM simulation. We find the subhaloes in 1 keV WDM have velocities up to 60% less than their CDM counterparts. This reduction decreases to 20% in 2 keV, 15% in 3 keV, and only 10% in 4 keV.

3.2.1 Velocity profiles

Figure 7 shows the NFW circular velocity profiles of the 10 subhaloes with the largest v_{max} at $z = 0$ in our WDM simulations after excluding Magellanic Cloud analogues.

The subhalo profiles are severely affected in the 1 keV cosmology with both the velocities and R_{max} values showing large changes. The 1 keV simulations struggle to match the observations in number and density with only *set D* managing to fit both.

Comparison to the CDM subhaloes plotted in Figure 5 shows some scatter among individual subhaloes. For example, a few subhaloes in *set B* have increased density in

WDM. In general, subhalo densities are significantly reduced in cosmologies warmer than 2 keV while at higher particle masses the effects are weak. This is in agreement with the single-halo simulations in Schneider et al. (2013) and Lovell et al. (2013).

4 DISCUSSION

We found the concentrations and velocity profiles of subhaloes in CDM simulations are dependent on the adopted cosmological parameters. We tested and found little to no dependence on the starting redshift, the mass resolution, the mass of the parent halo, and the halo finding software.

A cosmological dependence is also seen in other published work of Milky Way-sized galaxies. The simulations of Stoehr et al. (2002) used similar parameters to Aquarius, $(\Omega_m, \Omega_\Lambda, h, \sigma_8, n_s) = (0.3, 0.7, 0.7, 0.9, 1)$, and are well fit by Equation 3. di Cintio et al. (2011) saw an offset in their simulations using WMAP3 and WMAP5 parameters. A dependence of substructure central densities on the cosmological parameters is predicted in the work of Zentner & Bullock (2003) using the semianalytic model of Bullock et al. (2001). The central densities are expected to reflect the mean density of the universe at the time of collapse. Adopting values for cosmological parameters that moves the formation of small mass haloes to later epochs will result in less concentrated subhaloes.

Here we show how the subhalo densities can be simply related to the power at their mass scale and therefore dependent on both σ_8 and n_s . The parameter σ_8 sets the power at a scale of $8 \text{ Mpc } h^{-1}$ corresponding to a mass of about $2.5 \times 10^{14} M_\odot$. If the mass of the largest satellites is about $10^{10} M_\odot$, the wave number is $k_{sat} \sim 30k_8$ where k_8 is the wave number corresponding to $8 \text{ Mpc } h^{-1}$. The change in σ between WMAP3 and WMAP1 values of n_s is given by:

$$\frac{k_{sat}^{(n_s, WMAP3 - n_s, WMAP1)/2}}{k_8} \sim 0.92. \quad (4)$$

The change due to σ_8 is:

$$\frac{\sigma_{8, WMAP3}}{\sigma_{8, WMAP1}} \sim 0.82. \quad (5)$$

The total change at the satellites scale is $0.92 \times 0.82 = 0.76$. This is also proportional to the change of the redshift of formation:

$$(1 + z_f)_{WMAP3} = 0.76(1 + z_f)_{WMAP1}. \quad (6)$$

The virial radius is proportional to R_{max} at virialization and the circular velocity at the virial radius is proportional to v_{max} at virialization and:

$$R_{vir} \propto v_{vir}(1 + z_f)^{-1.5}. \quad (7)$$

Therefore we obtain the following scaling between cosmologies:

$$\frac{R_{max, WMAP3}}{R_{max, WMAP1}} = 0.76^{-1.5} = 1.51. \quad (8)$$

Repeating this for the scaling between Bolshoi and WMAP1 cosmologies yields a factor of 1.31. From our simulations we derived average scaling factors of 1.40 and 1.35 for WMAP3 and Bolshoi, respectively, with a scatter of 0.10. This is in good agreement with our rough calculation that assumes a

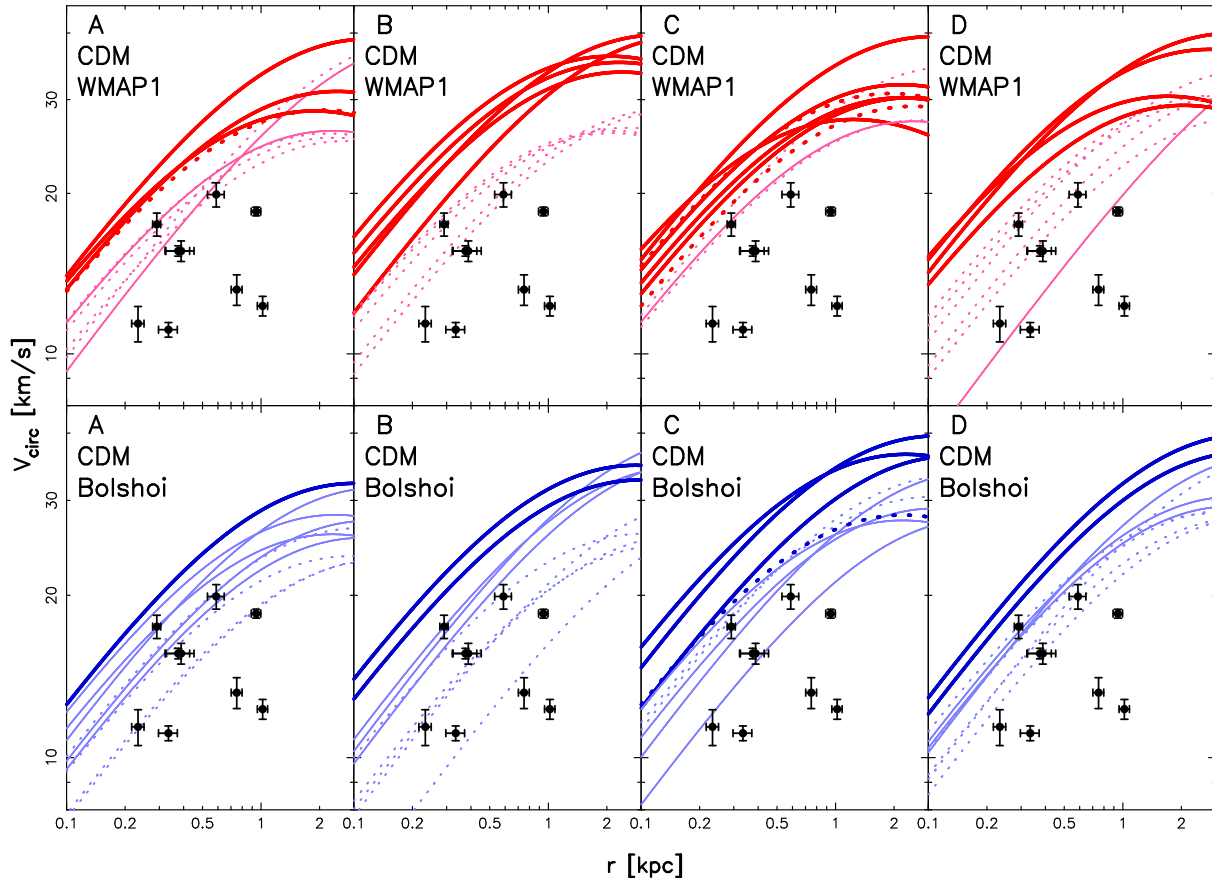


Figure 5. NFW circular velocity profiles for the 10 subhaloes with largest v_{max} at $z = 0$ in each CDM simulation adopting WMAP1 cosmology (*top row*); and Bolshoi cosmology (*bottom row*) after filtering Magellanic Cloud analogues. Subhaloes denser than any observed dwarf (points with error bars) are plotted in bold. Subhaloes that are neither among the 10 with largest v_{infall} or 10 largest v_{max} at $z = 9$ are not expected to host a bright dwarf and are plotted with dotted lines. Note that NFW profiles for the 10 subhaloes with largest v_{max} over their infall history select a few subhaloes with lower values of v_{max} and R_{max} than shown here, further alleviating the discrepancy with observations.

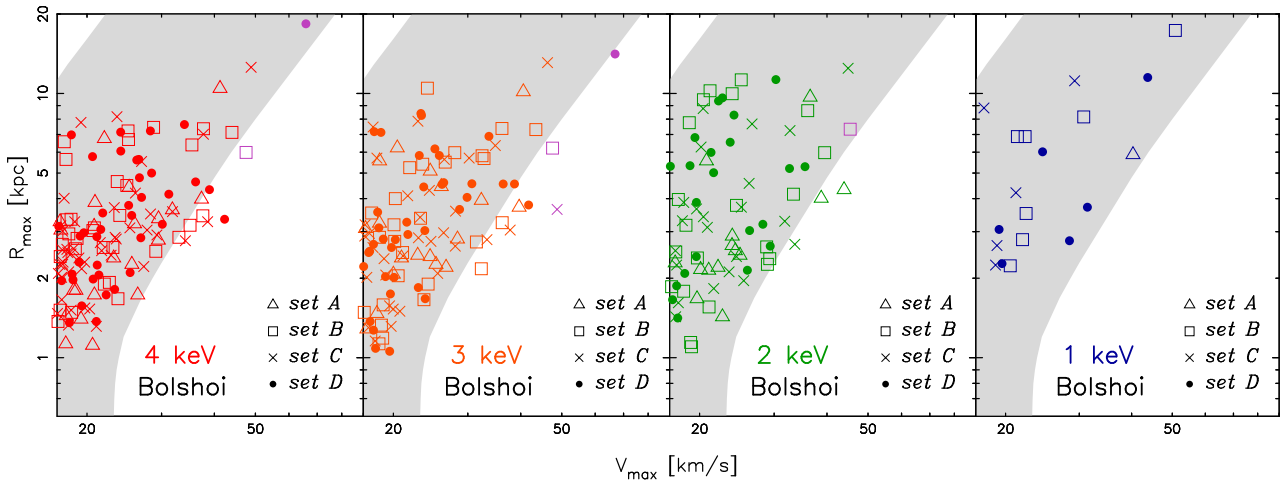


Figure 6. Plots of v_{max} and R_{max} for subhaloes in the high resolution WDM simulations adopting Bolshoi cosmological parameters. The shaded area shows the 2σ constraints for the bright Milky Way dwarfs assuming NFW profiles. Magellanic Cloud analogues are colored purple.

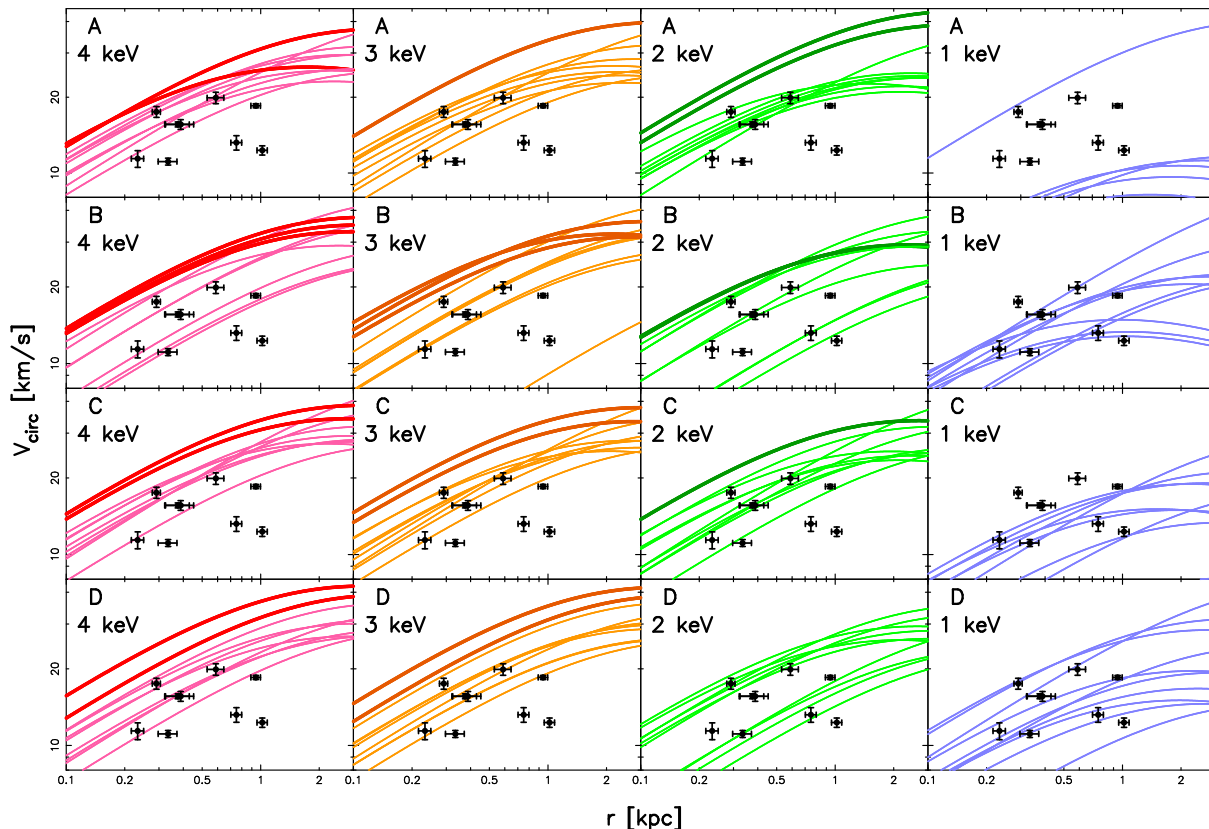


Figure 7. NFW circular velocity profiles for the 10 subhaloes with largest v_{max} at $z = 0$ in each WDM simulation adopting Bolshoi cosmology. Subhaloes denser than any observed dwarf (points with error bars) are plotted in bold.

mass of $10^{10} M_{\odot}$ for the large satellites and neglects tidal effects that may introduce a cosmology dependent change of the present values of R_{max} and v_{max} from the values at virialization. We can write an approximate general scaling relation for R_{max} at a fixed v_{max} :

$$R_{max} \propto (\sigma_8 5.5^{n_s})^{-1.5}. \quad (9)$$

This equation gives a scaling of 1.24 between Planck1 and WMAP1.

We also investigated how the subhalo densities are affected in a range of WDM cosmologies and quantified the reduction in circular velocity at kpc scales. In previous work we have shown (Polisensky & Ricotti 2011) that the abundance of Milky Way satellites, including the ultra-faint dwarfs discovered in the Sloan Digital Sky Survey, allow a lower limit of 2.3 keV to be placed on the dark matter particle mass. The work of Lovell et al. (2013) favors a similar but slightly warmer limit of 1.6 keV. Lyman- α absorption by neutral hydrogen along the line of sight to distant quasars over redshifts 2–6 probes the matter power spectrum in the mildly nonlinear regime on scales 1–80 Mpc h^{-1} . Several authors have used Lyman- α data to provide independent constraints on WDM with lower limits ranging from 1.7–4 keV (Boyersky et al. 2009; Viel et al. 2006; Seljak et al. 2006; Viel et al. 2008, 2013). Under these constraints we expect the circular velocities of the largest satellites in WDM to be affected by less than 20%, much less than the 60% changes seen in a 1 keV cosmology. We conclude that allowed WDM cosmologies have only a mild effect on the den-

sity of massive Milky Way satellites, that are instead most sensitive on the redshift of formation of the Milky Way and the power at small scales given by σ_8 and n_s .

While our simulations adopting Bolshoi cosmology reduced the number of “too big to fail” subhaloes in 3/4 of our Milky Way realizations from about four or five in WMAP1 to about one or two, none of our simulated Milky Ways are completely free of overdense subhaloes. Furthermore, the case of the VL2 halo demonstrates that large variation in average subhalo density is possible even in WMAP3 cosmologies. Purcell & Zentner (2012) examined 10,000 realizations of substructure for three host Milky Way masses from an analytic model. While their technique is only an approximation to direct simulation they find $\sim 10\%$ of their subhalo populations have no massive failures in a WMAP7 cosmology. The Milky Way may thus simply be mildly atypical. Interestingly, Hammer et al. (2007) show the Milky Way is deficient in stellar mass, disk angular momentum, and average iron abundance of stars in the Galactic halo at the 1σ level. Only $7\% \pm 1\%$ of spiral galaxies with comparable rotation speeds have similar properties. One way of explaining these discrepancies is to assume the Milky Way had a quiet accretion history without major merger events for the past ~ 10 Gyr. Figure 2 shows VL2 and our *set B* and *set C* haloes assemble $\sim 70\%$ of their mass by $z = 1.5$ and may better represent the Milky Way than the other haloes, according to this model. Opposite to expectations these haloes have the highest number of outliers. However, Purcell & Zentner

(2012) found selecting hosts for quiet accretion histories did not significantly increase the probability of consistency.

Our simulations assumed the dark matter was purely cold or purely warm, but a mixture of the two is possible. The transfer function of mixed dark matter is characterized by a step related to the particle mass and a plateau at smaller scales related to the fraction of the warm component. This could arise if the dark matter is composed of multiple particle species or a single species containing warm and cold primordial momentum distribution components caused by separate production stages, for example. Boyarsky et al. (2009) allowed for mixed cold and warm dark matter in their analysis of Lyman- α forest data. They find a particle mass of 1.1 keV is allowed if the WDM fraction is less than 0.4 (95% confidence). Masses below 1 keV are allowed provided the fraction of WDM is less than 0.35. Anderhalden et al. (2013) examined a subhalo population in several mixed dark matter cosmologies. They show a range of models that agree with Lyman- α constraints can be ruled out for failing to produce subhaloes with sufficient density to match the observations, highlighting the usefulness and uniqueness of the Milky Way satellites as a probe of small-scale cosmology.

ACKNOWLEDGMENTS

We thank Owen Parry for help running SUBFIND, Jürg Diemand for help accessing Via Lactea II data, and Michael Boylan-Kolchin for useful discussions. The simulations presented in this work were run on the DEEPTHOUGHT computing cluster at the University of Maryland College Park, the Cray XE6 GARNET at the U.S. Army Engineer Research and Development Center, the retired Cray XE6 RAPTOR and the SGI Ice X SPIRIT at the U.S. Air Force Research Laboratory. Basic research in astrophysics at NRL is funded by the U.S. Office of Naval Research. EP acknowledges support under the Edison Memorial Graduate Training Program at the Naval Research Laboratory. MR's research is supported by NASA grant NNX10AH10G and NSF CMMI1125285.

REFERENCES

- Anderhalden D., Schneider A., Macciò A. V., Diemand J., Bertone G., 2013, *JCAP*, 3, 14
- Bertschinger E., 2001, *ApJS*, 137, 1
- Bode P., Ostriker J. P., Turok N., 2001, *ApJ*, 556, 93
- Bovill M. S., Ricotti M., 2009, *ApJ*, 693, 1859
- Bovill M. S., Ricotti M., 2011a, *ApJ*, 741, 17
- Bovill M. S., Ricotti M., 2011b, *ApJ*, 741, 18
- Boyarsky A., Lesgourgues J., Ruchayskiy O., Viel M., 2009, *Phys. Rev. Lett.*, 102, 201304
- Boylan-Kolchin M., Bullock J. S., Kaplinghat M., 2011, *MNRAS*, 415, L40
- Boylan-Kolchin M., Bullock J. S., Kaplinghat M., 2012, *MNRAS*, 422, 1203
- Boylan-Kolchin M., Bullock J. S., Sohn S. T., Besla G., van der Marel R. P., 2012, *ArXiv e-prints*
- Bullock J. S., Kolatt T. S., Sigad Y., Somerville R. S., Kravtsov A. V., Klypin A. A., Primack J. R., Dekel A., 2001, *MNRAS*, 321, 559
- Bullock J. S., Kravtsov A. V., Weinberg D. H., 2000, *ApJ*, 539, 517
- Di Cintio A., Knebe A., Libeskind N. I., Brook C., Yepes G., Gottlöber S., Hoffman Y., 2013, *MNRAS*
- di Cintio A., Knebe A., Libeskind N. I., Yepes G., Gottlöber S., Hoffman Y., 2011, *MNRAS*, 417, L74
- Diemand J., Kuhlen M., Madau P., 2007, *ApJ*, 657, 262
- Diemand J., Kuhlen M., Madau P., Zemp M., Moore B., Potter D., Stadel J., 2008, *Nature*, 454, 735
- Eisenstein D. J., Hu W., 1998, *ApJ*, 496, 605
- Hammer F., Puech M., Chemin L., Flores H., Lehnert M. D., 2007, *ApJ*, 662, 322
- Hinshaw G. et al., 2012, *ArXiv e-prints*
- Jarosik N. et al., 2010, *ArXiv e-prints*
- Katz H., Ricotti M., 2012, *ArXiv e-prints*
- Klypin A., Kravtsov A. V., Valenzuela O., Prada F., 1999, *ApJ*, 522, 82
- Klypin A. A., Trujillo-Gomez S., Primack J., 2011, *ApJ*, 740, 102
- Knollmann S. R., Knebe A., 2009, *ApJS*, 182, 608
- Komatsu E. et al., 2009, *ApJS*, 180, 330
- Komatsu E. et al., 2011, *ApJS*, 192, 18
- Larson D. et al., 2010, *ArXiv e-prints*
- Lovell M. R. et al., 2012, *MNRAS*, 420, 2318
- Lovell M. R., Frenk C. S., Eke V. R., Jenkins A., Gao L., Theuns T., 2013, *ArXiv e-prints*
- Macciò A. V., Dutton A. A., van den Bosch F. C., 2008, *MNRAS*, 391, 1940
- Moore B., Ghigna S., Governato F., Lake G., Quinn T., Stadel J., Tozzi P., 1999, *ApJ*, 524, L19
- Navarro J. F., Frenk C. S., White S. D. M., 1997, *ApJ*, 490, 493
- Planck Collaboration et al., 2013, *ArXiv e-prints*
- Polisensky E., Ricotti M., 2011, *Phys. Rev. D*, 83, 043506
- Power C., Navarro J. F., Jenkins A., Frenk C. S., White S. D. M., Springel V., Stadel J., Quinn T., 2003, *MNRAS*, 338, 14
- Purcell C. W., Zentner A. R., 2012, *JCAP*, 12, 7
- Ricotti M., Gnedin N. Y., 2005, *ApJ*, 629, 259
- Ricotti M., Gnedin N. Y., Shull J. M., 2002a, *ApJ*, 575, 33
- Ricotti M., Gnedin N. Y., Shull J. M., 2002b, *ApJ*, 575, 49
- Ricotti M., Gnedin N. Y., Shull J. M., 2008, *ApJ*, 685, 21
- Sawala T., Frenk C. S., Crain R. A., Jenkins A., Schaye J., Theuns T., Zavala J., 2012, *ArXiv e-prints*
- Schneider A., Anderhalden D., Maccio A., Diemand J., 2013, *ArXiv e-prints*
- Seljak U., Makarov A., McDonald P., Trac H., 2006, *Phys. Rev. Lett.*, 97, 191303
- Spergel D. N. et al., 2007, *ApJS*, 170, 377
- Spergel D. N. et al., 2003, *ApJS*, 148, 175
- Springel V., 2005, *MNRAS*, 364, 1105
- Springel V. et al., 2008, *MNRAS*, 391, 1685
- Springel V., White S. D. M., Tormen G., Kauffmann G., 2001, *MNRAS*, 328, 726
- Stoehr F., White S. D. M., Tormen G., Springel V., 2002, *MNRAS*, 335, L84
- Vera-Ciro C. A., Helmi A., Starkenburg E., Breddels M. A., 2013, *MNRAS*, 428, 1696
- Viel M., Becker G. D., Bolton J. S., Haehnelt M. G., 2013, *Phys. Rev. D*, 88, 043502
- Viel M., Becker G. D., Bolton J. S., Haehnelt M. G., Rauch M., Sargent W. L. W., 2008, *Phys. Rev. Lett.*, 100, 041304

- Viel M., Lesgourgues J., Haehnelt M. G., Matarrese S., Riotto A., 2006, *Phys. Rev. Lett.*, 97, 071301
- Vogelsberger M., Zavala J., Loeb A., 2012, *MNRAS*, 423, 3740
- Walker M. G., Mateo M., Olszewski E. W., Peñarrubia J., Wyn Evans N., Gilmore G., 2009, *ApJ*, 704, 1274
- Wang J., Frenk C. S., Navarro J. F., Gao L., Sawala T., 2012, *MNRAS*, 424, 2715
- Wolf J., Martinez G. D., Bullock J. S., Kaplinghat M., Geha M., Muñoz R. R., Simon J. D., Avedo F. F., 2010, *MNRAS*, 406, 1220
- Zentner A. R., Bullock J. S., 2003, *ApJ*, 598, 49
- Zolotov A. et al., 2012, *ApJ*, 761, 71